Pain Control on Demand Based on Pulsed Radio-Frequency Stimulation of the Dorsal Root Ganglion Using a Batteryless Implantable CMOS SoC

Hung-Wei Chiu, Mu-Lien Lin, Chii-Wann Lin, I-Hsiu Ho, Wei-Tso Lin, Po-Hsiang Fang, Yi-Chin Lee, Yeong-Ray Wen, and Shey-Shi Lu, *Senior Member, IEEE*

***Abstract*—This paper presents the implementation of a batteryless CMOS SoC with low voltage pulsed radio-frequency (PRF) stimulation. This implantable SoC uses 402 MHz command signals following the medical implanted communication system (MICS) standard and a low frequency (1 MHz) for RF power transmission. A body floating type rectifier achieves 84% voltage conversion ratio. A bi-phasic pulse train of 1.4 V and 500 kHz is delivered by a PRF driver circuit. The PRF parameters include pulse duration, pulse frequency and repetition rate, which are controllable via 402 MHz RF receiver. The minimal required 3 V RF V_{in} and 2.2 V V_{DDr} is achieved at 18 mm gap. The SoC chip is fabricated in a 0.35 μm CMOS process and mounted on a PCB with a flexible spiral antenna. The packaged PRF SoC was implanted into rats for the animal study. Von Frey was applied to test the mechanical allodynia in a blinded manner. This work has successfully demonstrated that implanted CMOS SoC stimulating DRG with 1.4 V, 500 kHz PRF could significantly reduce spinal nerve ligation (SNL) induced mechanical allodynia for 3–7 days.**

***Index Terms*—Batteryless, dorsal root ganglion, implantable, pain control, pulsed radio frequency.**

I. Introduction

ALTHOUGH pain is interpreted as the fifth vital sign, the presence of different degrees of pain significantly affects quality of life for many patients, especially the elderly [1]. Low back pain (LBP) is also the fifth most common reason for all physician visits in the U.S. [2], [3]. Approximately 40% of LBP sufferers have neuropathic pain [4], which may result from inflammation of the dorsal root ganglia (DRG) due to compression by herniated intervertebral disc disease or intervertebral foramen stenosis [5]–[7]. Electrical stimulation to the central or peripheral neural conduction paths has been utilized in clinics to achieve effective pain relief [8], such as electroacupuncture therapy, interferential wave therapy, peripheral electrical nerve stimulation (PENS) [9] transcutaneous electrical nerve stimulation (TENS), etc.

The conventional continuous radio-frequency (CRF) pain therapy uses thermal coagulation to permanently damage nerves by high-temperature ablation of nerve tissues. This destructive method can cause severe side effects, such as the de-aferentation pain [8]. Thus, repeated surgery is needed. In 1988, the pulsed radio frequency (PRF) was developed to replace the conventional CRF [10]. Instead of the thermal lesion, electrical stimulation was applied to minimize thermal damage. The basic principal of electrical stimulation is based on "gate theory" [11], blocking the signal of pain conduction with nondestructive spinal cord stimulation.

It is found that repetitive burst-like electrical stimulation of A-delta fibers caused depression of synaptic activation by C-fiber for several hours [12]. Pulsed radio-frequency (PRF) may inhibit C-fiber excitatory responses [13]. And the analgesic action of PRF involves the enhancement of noradrenergic and serotonergic descending pain inhibitory pathways [14]. It was suggested that radicular pain is caused by irritation of DRG. Many clinical reports have largely involved treatment of neuropathic pain condition, with treatment regimens using PRF applied close to the DRG [15]–[17]. Clinical experiments have reported pain relief sustains for weeks to months after PRF treatment. It was also reported the clinical effectiveness of PRF up to 90% [18]. Yet, the overall clinical evidence of PRF is still weak and the duration of maintaining the effectiveness is short. The LBP recurred every 3–6 months in average after PRF therapy [19]–[21], which caused the chronic LBP patient troublesome.

Thus, PRF is known for its inconvenience of short-term effectiveness on pain relief. Hence, an implantable PRF treatment is proposed to overcome this issue in this paper. The conventional implantable system requires a battery for operation, often

Manuscript received June 12, 2010; revised September 06, 2010; accepted September 21, 2010. Date of publication November 11, 2010; date of current version November 24, 2010. This work was supported in part by the National Science Council (NSC) of R.O.C., Taiwan under Contracts NSC97-2221E-002240, NSC97-2623E-002003IT, NSC97-2221E-002153-MY3, and NSC 98-2221-E-027075, and in part by the Ministry of Economic Affairs under Contract MOEA98-EC-17-A-07-S2-0123. This paper was recommended by Associate Editor H.-J. Yoo.

H.-W. Chiu and I.-H. Ho are with the Department of Electronic Engineering and Graduate Institute of Computer and Communication Engineering, National Taipei University of Technology, Taipei 10608, Taiwan (e-mail: hwchiu@ntut.edu.tw).

M.-L. Lin is with the Institute of Biomedical Engineering, National Taiwan University, Taipei 10616. He is also with the Zhongxing Branch of Taipei City Hospital, Taipei 103 (e-mail: linmulien@yahoo.com.tw).

C.-W. Lin and W.-T. Lin are with the Institute of Biomedical Engineering, National Taiwan University, Taipei 10616, Taiwan (e-mail: cwlinx@ntu.edu.tw).

P.-H. Fang, Y.-C. Lee, and S.-S. Lu are with are with the Graduate Institute of Electronics Engineering, National Taiwan University, Taipei 10617, Taiwan (e-mail: sslu@ntu.edu.tw).

Color versions of one or more of the figures in this paper are available online at http://ieeexplore.ieee.org.

Digital Object Identifier 10.1109/TBCAS.2010.2081668

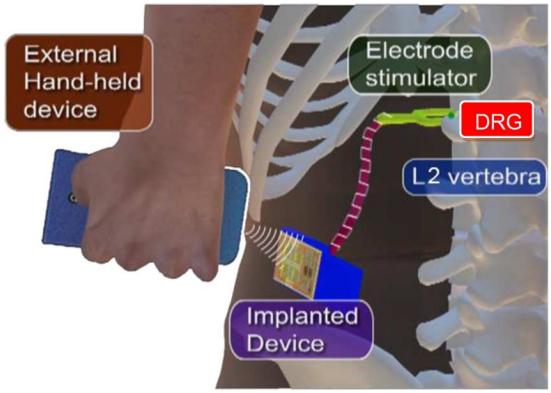

Fig. 1. DRG stimulation for pain relief.

accounting for over 2/3 of the entire device volume. Therefore, a non-destructive and batteryless method using PRF for pain control is the key for implantable systems. This work proposes a novel batteryless implantable pain control SoC that is effective in pain relief, using a low voltage stimulation e which avoids causing thermal damage to dorsal root ganglion (DRG) tissue. As illustrated in Fig. 1, this system provides the self-controlled analgesia for low back pain through adjustment of PRF parameters by external handheld device. An animal study of neuropathic pain was previously designed with PRF parameters to control tissue temperature at $< 40\,^{\circ}\mathrm{C}$ via an external function generator [21]. Here, this work presents for the first time the implementation of such functionality on a complementary metal–oxide semiconductor (CMOS) system-in-a-chip (SoC). Its effectiveness is demonstrated by observing the behavior of rats receiving localized bipolar low-voltage stimulus to the DRG of lumbar spine.

II. System Architecture

A. Circuit Blocks

Fig. 2 shows a system block diagram of the proposed CMOS SoC consisting of a radio frequency to direct current (RF-dc) circuit, a voltage limiter, regulators, an RF receiver, a clock regenerator, a logic controller and a PRF driver. This implantable SoC uses 402 MHz command signals following the medical-implanted communication system (MICS) standard and a low frequency (1 MHz) spiral antenna size for easy user alignment and increased penetration depth. The RF-dc circuit receives power from an external 1 MHz RF power source located outside the skin. This circuit converts the RF signal into a dc voltage $\mathrm{V_{DDr}}$. The following voltage limiter limits the dc voltage to a maximum of 5 V, which can be regulated by two regulators. One regulates $\mathrm{DV_{DD}}$ for the digital circuit, which is adjusted by an external resistor. One regulates $\mathrm{AV_{DD}}$ to 1.8 V for the analog circuit. The clock regenerator, which is a Schmitt trigger circuit, regenerates the 1 MHz as system clock. It extracts the clock signal from the RF source for the logic controller. The PRF generator of logic controller makes default biphasic PRF waveforms for the PRF drivers. In addition to the default parameters (a pulse train with a period of 50 ms modulated by a 500-kHz carrier), users can specify a custom stimulation protocol in the logic controller via a handheld device. To generate the biphasic PRF waveform, the output of the PRF generator is split into two paths. One signal of the paths is delayed by one clock cycle. The PRF drivers, each consisting of three cascaded inverters that increase driving capability, can generate output voltages in the range of 1.4 V to 3.3 V. Both electrodes are placed into the surgically exposed L5 nerve of the lumbar region for stimulus in the animal studies. Furthermore, the RF on-off keying (OOK) receiver receives external commands from a personal computer (PC) or personal data assistant (PDA) and directs the logic controller to output the specified PRF waveform.

B. RF-DC

The RF-DC is a conventional two-way rectifier circuit composed of 2 nMOS and 2 pMOS [23]. The nMOS transistors (10000 μm/0.5 μm) perform current switching function, which achieve low power loss due to the low $\mathrm{r_{ds}}$ of nMOS, when rectifying. However, an nMOS switching network can't coexist with a pMOS switching network. Because a switch conducts current in both directions, it would generate an unwanted reverse current when switching. By using the diode connected pMOS transistors to pass current directionally as shown in Fig. 3, the reverse current is stopped. Note that the nMOS transistors are tied to gound via substrate resistor $\mathrm{R_{sub}}$. The bodies of the 2 pMOS transistors are weakly tied to $\mathrm{V_{DDr}}$ by the additional resistor $\mathrm{R_{bp}}$.

If the body of the diode connected pMOS transistor is directly connected to the $\mathrm{V_{DDr}}$ without $\mathrm{R_{bp}}$, the MOS diode is in the same direction parallel with the intrinsic body diode. By proper connections as shown in Fig. 4, the individual IV characteristics of the MOS diode and the body diode were measured. It shows that the MOS diode has lower cut-in voltage than the body diode. Although the body diode has a better conductivity for larger current, it also suffers from severe reverse recovery current when switching. The reverse recovery current not only degrades the efficiency but also generates power supply noise at $\mathrm{V_{DDr}}$. Besides, the needed operating current for the following circuit is less than 5 mA. The MOS diode will dominate the conducting current. Hence, $\mathrm{M_{P1}}$ and $\mathrm{M_{P2}}$ are connected to $\mathrm{V_{DDr}}$ by $\mathrm{R_{bp}}$ (10 kΩ) to avoid body diodes. 1 MHz sine wave with 5 V amplitude was rectified to be 4.2-V dc output with $C_L = 1$ nF and $R_L = 1$ kΩ. The voltage conversion ratio $V_{DD}/|V_{in}|$ of the individual RF-dc circuit is about 84% [24].

C. Voltage Limiter and Regulator

As shown in Fig. 5(a), $\mathrm{Z_P}$ is a virtual resistor representing the load from the implanted device via the coupling spiral antenna. If the resistive load in the secondary side is $\mathrm{R_C}$, the feedback input impedance from the primary side is derived

$$\mathrm{Z_P} = \frac{\mathrm{sL_P R_C} + \mathrm{s^2 L_P L_S}(1-\mathrm{K^2}) + \mathrm{s^3 L_P L_S C_S R_C}(1-\mathrm{K^2})}{\mathrm{R_C} + \mathrm{sL_S} + \mathrm{s^2 L_S C_S R_C}}. \quad (1)$$

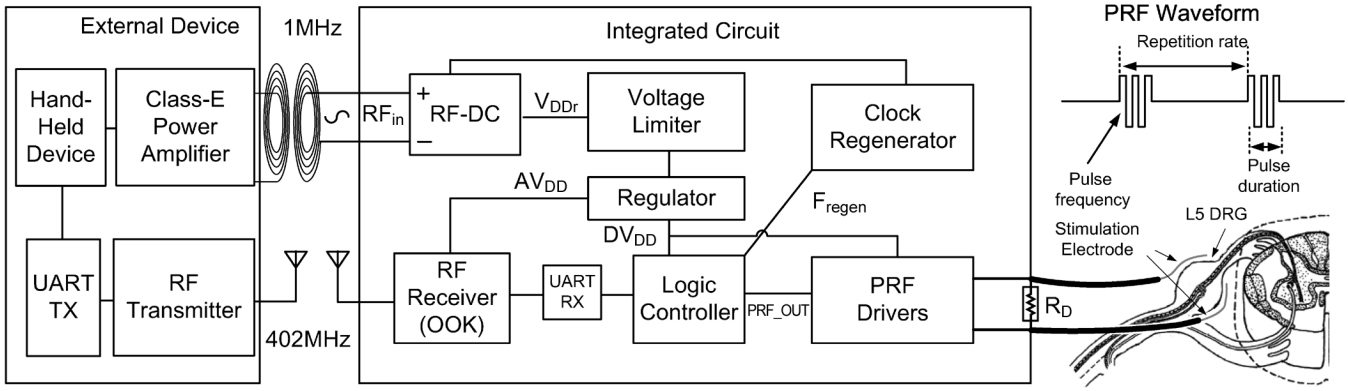

Fig. 2. System block diagram of the implantable DRG stimulator for pain control.

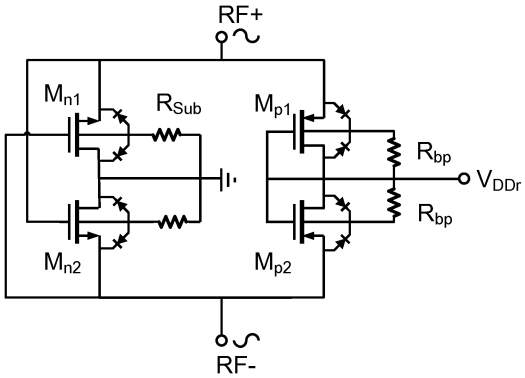

Fig. 3. Schematic of proposed full-wave rectifier.

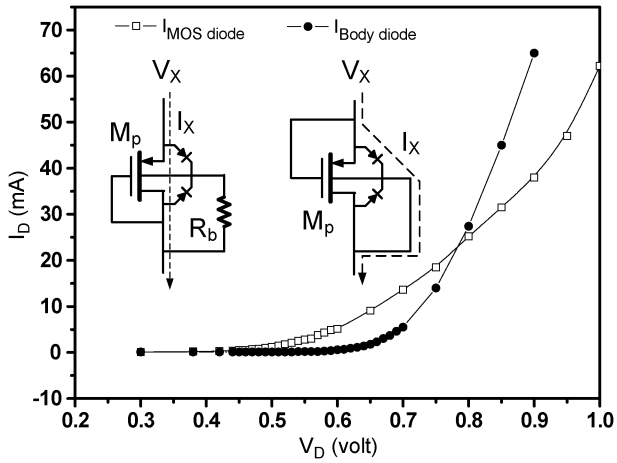

Fig. 4. IV curve comparison of MOS diode and body diode.

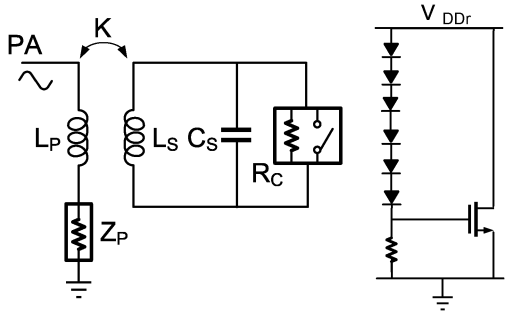

Fig. 5. (a) Inductive coupling circuit model of the voltage limiter. (b) Schematic diagram of voltage limiter.

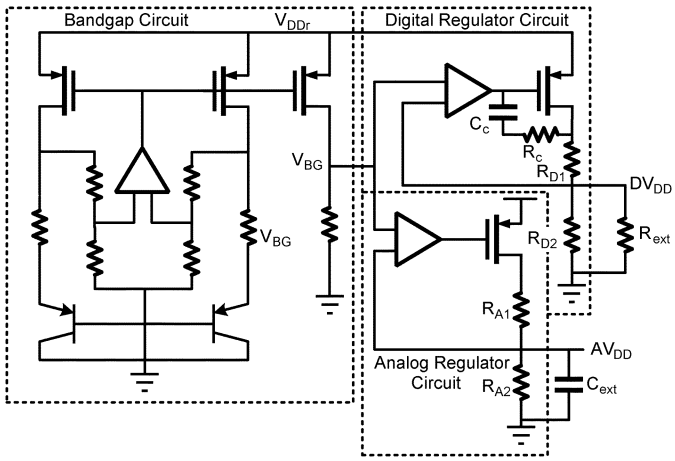

Fig. 6. Schematic diagram of the regulators which generate $\mathrm{DV_{DD}}$ and $\mathrm{AV_{DD}}$.

If resonating in the secondary part, $\mathrm{sL_s} + (1/\mathrm{sC_s}) = 0$. The $\mathrm{Z_P}$ is reduced as

$$\mathrm{Z_P} = \mathrm{sL_p}(1-\mathrm{K^2}) + \frac{\mathrm{L_p}}{\mathrm{L_s}}\mathrm{R_C}\mathrm{K^2} = \mathrm{sL_p}(1-\mathrm{K^2}) + \mathrm{NR_C}\mathrm{K^2} \quad (2)$$

where N is defined as the ratio of $\mathrm{L_P}$ and $\mathrm{L_S}$. If $\mathrm{K} = 1$ and $\mathrm{L_P} = \mathrm{L_S}$, $\mathrm{Z_P}$ becomes equal to $\mathrm{R_C}$ and $\mathrm{L_P}$ vanishes. Note that the real part of $\mathrm{Z_P}$, which is defined as $\mathrm{R_P}$, is proportional to $\mathrm{K^2}$ value.

The voltage sensor in the voltage limiter is composed of 5 serial connection diodes and a 200-kΩ resistor, which is plotted in Fig. 5(b). When the input voltage exceeds 5 V, it will turn on the nMOS transistor to pull down the current from the power source. Since the pulled down current could be large, the size of the MOS is up to 4000 μm/0.35 μm. As shown in Fig. 5(a), it causes short-circuit load on the secondary side. With this, zero $\mathrm{R_C}$ is fed back, $\mathrm{Z_P}$ becomes zero that limits the RF power immediately and suppresses the received voltage.

If the rectified $\mathrm{V_{DDr}}$ is lower than 5 V, the voltage limiter is quiescent and the following voltage regulator uses this voltage to generate a regulated operating voltage for analog and digital

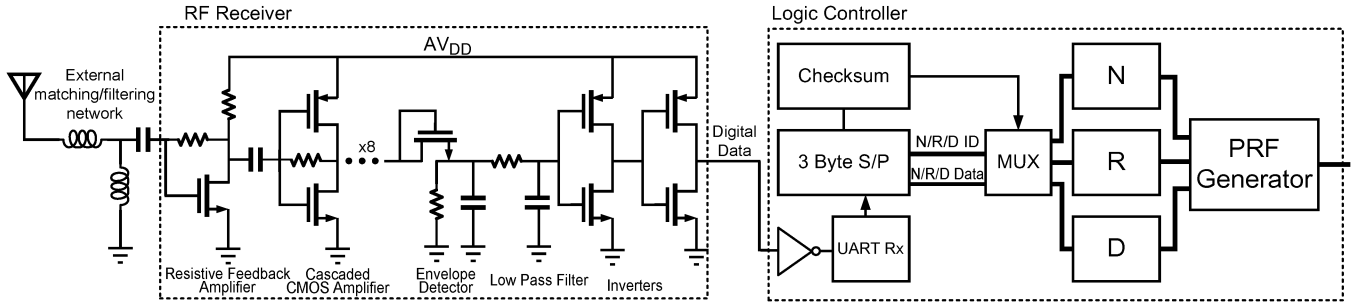

Fig. 7. Schematic diagram of the OOK receiver [25].

circuits as shown in Fig. 6. The digital and analog regulators use the same bandgap reference [19]. The analog circuit is mainly composed of a low-voltage RF receiver circuit, which operates at 1.8 V. Since the rectified $\mathrm{V_{DDr}}$ still carries large RF power noise, a large external 100 μF, $\mathrm{C_{ext}}$ is necessary to filter out the RF power noise. Besides, this large output capacitor also helps compensating the stability of regulator. As to the digital circuit, it is not sensitive to the RF power noise, a large $\mathrm{C_{ext}}$ is unnecessary for the digital regulator. A default $\mathrm{DV_{DD}}$ is also 1.8 V without the external discrete resistor $\mathrm{R_{ext}}$. In order to study the effect of the PRF operating voltage, the $\mathrm{DV_{DD}}$ is adjustable by adding additional $\mathrm{R_{ext}}$.

D. RF Receiver

This system provides not only a self-controlled analgesia for the low back pain, but also the therapy of PRF parameters is also controllable. The self-therapy PRF parameters defined by the user are wirelessly transmitted at 402 MHz. Conventionally, an implantable device can use the same inductively power coupling path to carry data. In this system, we propose separate power and data path so that the data transmission distance can be longer once a battery is equipped. Fig. 8 defines the format of the self-therapy PRF parameters data packet in which the first byte is N/R/D ID and the following byte defines N/R/D data, which are responsible for pulse frequency, repetition rate and pulse duration parameters. The last byte is the sum of previous two bytes and defined as Checksum. The parameters are set in the handheld device, which UART is almost available. In general, TX is kept at high voltage when standby. In order to save power consumption, the TX output is inverted first and then sent to RF OOK transmitter. Therefore, RF transmitter is OFF when no data is sent and TX is in standby. If those parameters are not available in the implanted device, the hard-wired default N/R/D in the logic controller will activate for normal operation.

When the parameters are set and activated in the handheld device, a 3-B data packet is formed and sent via UART TX port and the following RF transmitter.

Due to the low data rate and short transmission distance, a simple OOK modulation scheme is chosen for low power consumption and small size [26]. The OOK receiver always listens to 402 MHz for the incoming packet. This RF block is fed by $\mathrm{AV_{DD}}$ which is regulated at 1.8 V. As shown in Fig. 7, the first stage in the integrated OOK receiver is a resistive shunt-shunt feedback amplifier with high input impedance, which is connected to an external matching/filtering network. The following

1Byte	1Byte	1Byte
N/R/D ID	N/R/D Data	Checksum

Fig. 8. Format of self-therapy PRF parameters data packet.

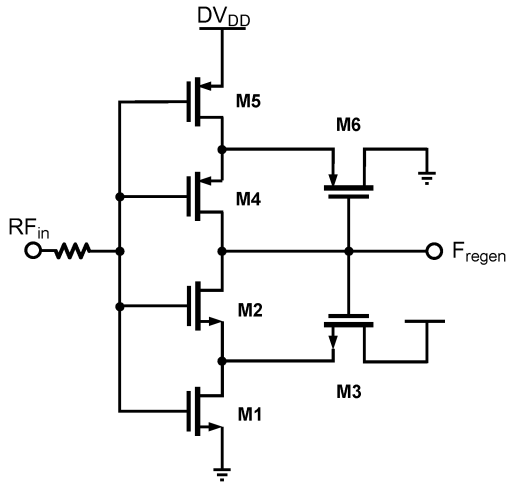

Fig. 9. Schematic diagram of clock regenerator.

gain stage is an eight-stage cascaded CMOS amplifier. These two amplifiers provide 60-dB gain in total. The data are demodulated by the envelope detector and the low-pass filter, which is composed of an integrated 1-kΩ resistor and a 10-pF capacitor. The final inverters are used to shape the modulated signal into digital output. Once the RF signal is received by the RF receiver, it is directly demodulated into the digital packet and handheld by UART RX. The serial data are then converted to parallel by the S/P circuit and is used to calculate the checksum. If the serial data are verified correct, the MUX would pass the N/R/D data to the relative N/R/D registers according to the N/R/D ID. Once these parameters are available in the registers, the PRF generator would immediately process data and change the PRF waveform.

E. Logic Circuits for PRF Generator and PRF Drivers

The 1-MHz system clock of a logic controller is captured from the RF power signal by the clock regenerator, which is a Schmitt trigger as shown in Fig. 9. It offers better noise immunity and noise margin. Moreover, its operating voltage can be as low as 1.7 V.

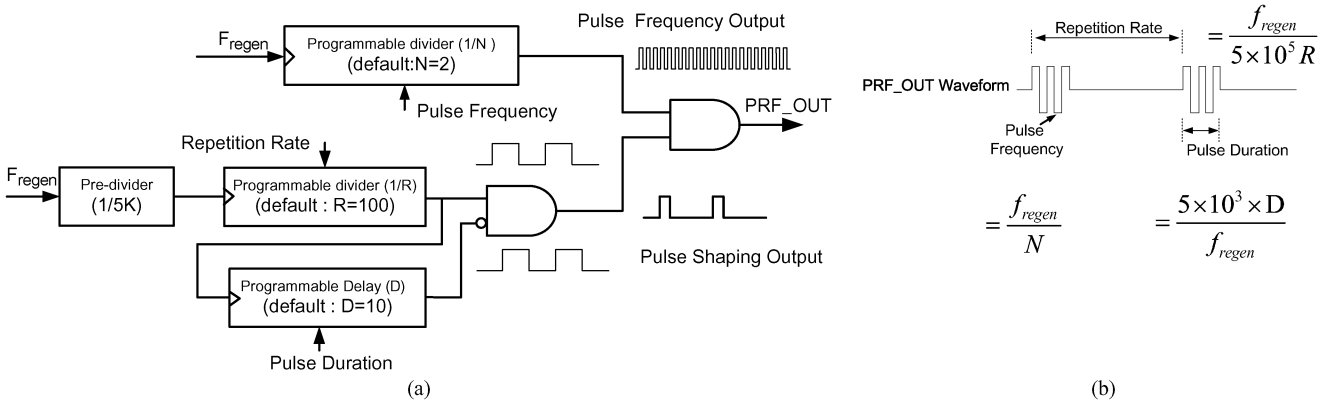

Fig. 10. (a) Block diagram of the PRF generator. (b) PRF waveform and parameters definition.

The basic PRF parameters consist of pulse frequency, repetition rate and pulse duration, which are defined in Fig. 10(b). The base frequency originates from the regenerated clock $(\mathrm{F_{regen}})$. The programmable divider circuit divides the $\mathrm{F_{regen}}$ by N and generates the pulse frequency output. If N is not set by the external RF signal command, the default N is 2 and the default pulse frequency is 500 kHz. As shown in Fig. 10(a), the PRF output waveform is shaped by the pulse-shaping output, which is the result of AND gate. The repetition rate of the pulse train is default 2 Hz with default $\mathrm{R} = 100$. Pulse duration is controlled by programmable delay D, which delays the output of the repetition rate output by D times the predivider output clock. The default $\mathrm{D} = 10$ generates 50-ms delay. All three programmable parameters can be reset by the RF receiver.

The ready PRF waveform is then delivered to PRF drivers. In order to double the stimulating voltage, the differential PRF outputs can be easily produced by the 3-stage and 4-stage inverter chains as shown in Fig. 11(a). However, the nonzero dc level in the quiescent period of PRF is observed. It causes a long period of dc current passing through the nerve and may bring thermal damage. Besides, the dc level in the course of the pulse train is zero and is different from the quiescent period. Consequently, charges in the nerve become unbalanced between pulse train and quiescent time. The charge unbalance did cause the rat leg jerking. Only the operated side of the leg jerked with the frequency of 2 Hz, which is the same with the repetition rate. Although this inverting-type driver has an unsafe effect for living creatures, it helps the surgery to have a visible response for positioning.

The charge balance stimulation is achieved in Fig. 11(b). It shows that the positive node leads the negative node by one clock cycle. Thus, the dc level would be almost zero in the whole period of stimulation. This delay type driver did not cause jerking. As shown in Fig. 11(c), the inverter chain is an effective and easy circuit to drive the PRF waveform for nerve stimulation. The geometric ratio of the inverter size is 2. Unlike the analog driving circuit, the digital inverter can deliver a constant voltage of $\mathrm{DV_{DD}}$ but not a constant current. The voltage across the nerve would be positive or negative $\mathrm{DV_{DD}}$ alternatively. Hence, it is square waveform stimulation. Therefore, the most part of the current flowing through the nerve is dc current. Hence, the imaginary part of the nerve is ignored. Since

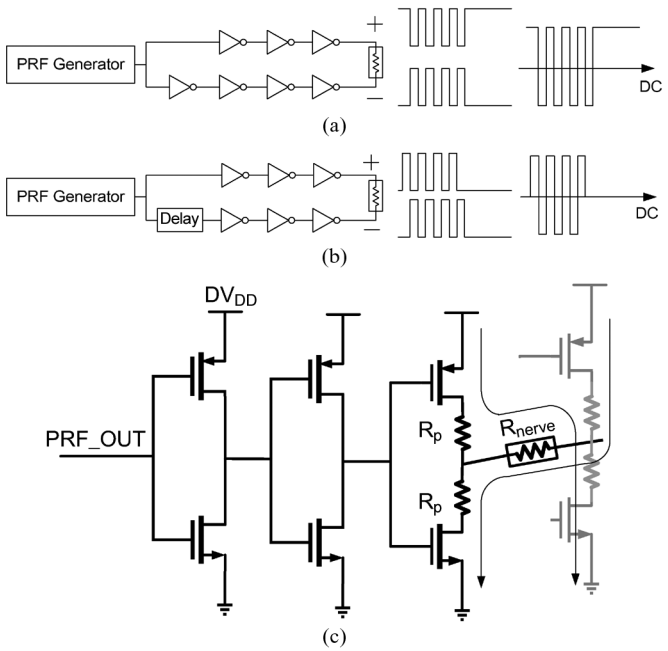

Fig. 11. (a) Inverting-type PRF driver. (b) Delayed-type PRF driver. (c) Current flow of biphasic PRF.

the impedance of the stimulated nerve is uncertain, the maximal current must be limited for safety. Two 50-Ω resistors are connected between the output node and the source of transistors. The measured the output current with respect to the $\mathrm{R_{nerve}}$ is plotted in Fig. 12. A common $\mathrm{R_{nerve}}$ is around 1 kΩ. If the $\mathrm{R_{nerve}}$ is 1 kΩ and $\mathrm{DV_{DD}}$ is regulated at 1.4 V, the measured output current is 1.22 mA. In case $\mathrm{R_{nerve}}$ becomes 10 Ω unexpectedly, the output current would be limited at 12.5 mA.

III. Measured Results

This pain control chip is fabricated in a 0.35-μm CMOS process. Fig. 13 shows the die micrograph of the proposed pain control chip whose size is 2.1 mm $\times$ 2.2 mm. Over half of the size is occupied by the rectifier in order to enhance its efficiency and reduce thermal effect. This chip is mounted on a printed-circuit board (PCB), which is connected to a flexible spiral antenna. Fig. 14 shows the stimulator module, whose dimension is 1.5 cm wide $\times$ 4 cm long $\times$ 5 mm high. While the

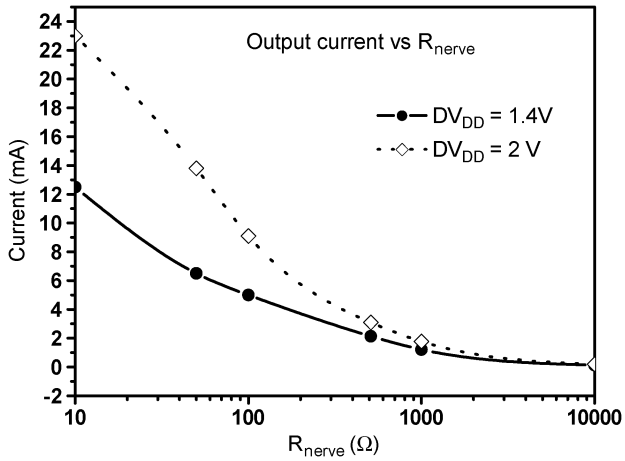

Fig. 12. PRF driving current with respect to different impedance values.

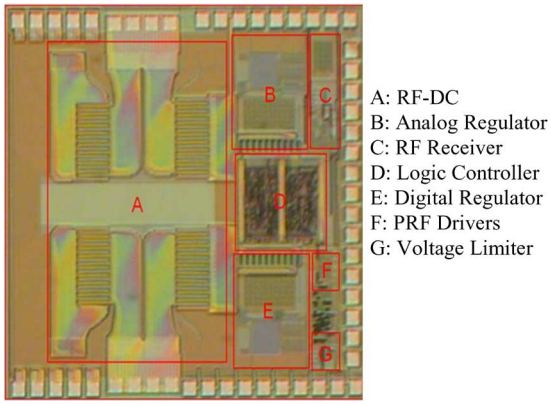

Fig. 13. Micrograph of the pain control IC.

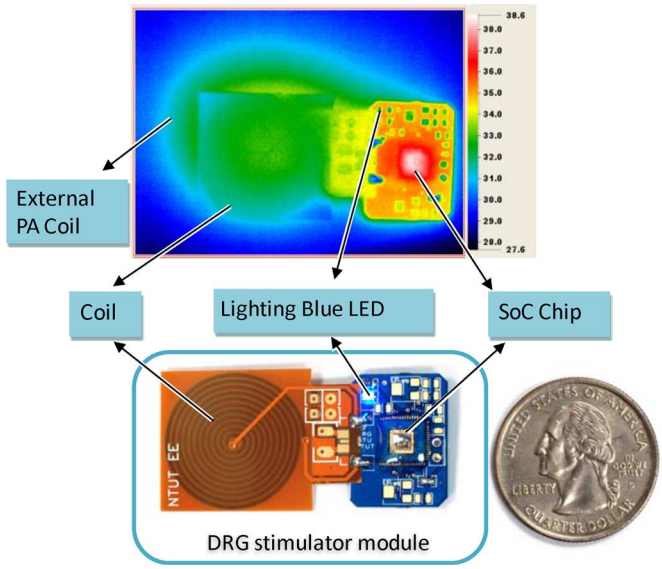

Fig. 14. DRG stimulator module and its measured IR thermography when activated.

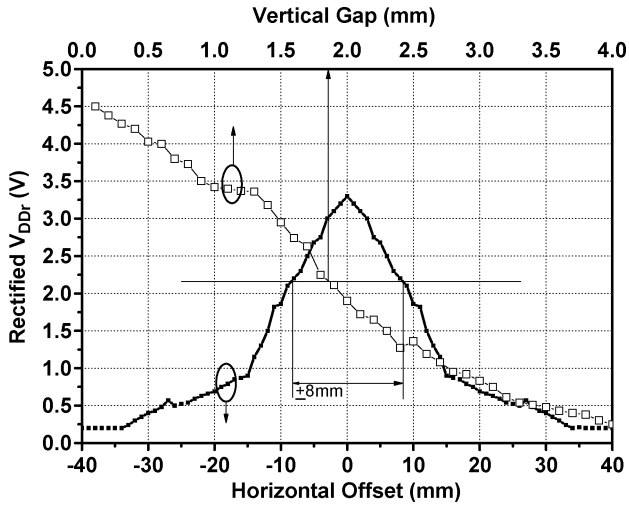

Fig. 15. Rectified V_{DDr} with respect to the vertical and horizontal offset.

flexible spiral antenna is folded, the module becomes half-size, which is as small as a U.S. quarter.

Before implantation, the operating temperature was measured by an infrared (IR) thermal imager to ensure the thermal biocompatibility for the *in vivo* experiment. When the thermography was taken, the DRG stimulator was placed under the coil of PA without any vertical gap and horizontal offset. The IR thermography in Fig. 14 shows that the highest temperature 39 °C occurs in the chip. These two IR thermography and photograph with a blue light-emitting diode (LED) lightning were taken at the same time. Since this coupling is the closest condition, the operating temperature of the module should be below the maximal 39 °C when implanted. Besides, the temperature of these two spiral antennas is also observed that heat is also generated by the antennas. It arises from the low Q spiral antennas, whose Q was also measured at about 5.5 at 1 MHz by a network analyzer.

In order to study the RF powering, rectified V_{DDr} was measured with respective to the inductive contact alignment when the VDD of Class-E PA was 6 V. Fig. 15 shows that the highest rectified V_{DDr} is 4.5 V when using the direct contact without any gap. V_{DDr} degrades with the increase of the gap distance. The minimal required V_{DDr} is 2.2 V, which corresponds to the maximal 18-mm gap distance. This distance is enough for implanting under the skin. In addition, V_{DDr} versus the horizontal offset was also measured with a 10-mm distance of the gap. That means when the module implantation is 10 mm deep, the maximal alignment offset of the antenna center is about ±8 mm. To achieve the minimal operating DV_{DD} 1.4 V, the minimal input V_{RF} amplitude should be larger than 3 V to deliver a rectified 2.2 V V_{DDr} with 2.7-mA operating current. When connected to a 1.6 kΩ resistive load, which was the measured DRG impedance, the PRF driver delivers an output 1.3-V PRF waveform, which is lower than 1.4 V DV_{DD} due to the current protection resistor R_p. PRF waveforms with different periods (0.05 to 1.25 s) and different modulation frequencies (4 kHz to 1 MHz) can be measured successfully. Table I summarizes the characteristics of the proposed SoC, along with those of other implantable electrical stimulators [27]–[30].

IV. Animal Study Method and Results

The whole module was packaged by PDMS for water proof and humidity sealing. Besides, it was coated with biocompatible

TABLE I
SUMMARY OF THE MEASURED PERFORMANCE

	This work	Ref[27]	Ref[28]	Ref[29]	Ref[30]
Application	Pain control (DRG)	Pain Control (Epi-dura)	FES*	BCI**	DBS+
Battery	No	Yes	No	No	Yes
Animal study	Yes	Yes	Yes	No	No
Technology	0.35 μm CMOS	N/A	Off-chip RLC	1.5 μm CMOS	0.18 μm CMOS
RF-DC efficiency(max)	80%	No RF-DC	N/A	N/A	No RF-DC
Minimal V_{DDr}	2.4V	No RF-DC	N/A	N/A	No RF-DC
Power source frequency	1 MHz	No RF Powering	480 kHz	5/10 MHz	No RF Powering
RF receiver frequency	402 MHz	No wireless transmission	480 kHz	5/10 MHz	No wireless transmission
Transmission distance	< 1.8 cm	No wireless transmission	N/A	0.5cm	No wireless transmission
Full scale output	>2.8 V	10.5 V	30 mA	250 μA	135 μA
PRF output power (Rd = 1.5 kΩ)	1.12 mW	N/A	N/A	N/A	N/A
Chip temperature	< 39 ℃	N/A	N/A	N/A	N/A
Stimulation mode	PRF (Reconfigurable)	Continuous	Continuous	Continuous	Continuous
Pulse frequency	4 kHz ~ 1 MHz	2~1200 Hz	480 kHz	N/A	N/A
Pulse duration	0.05~ 1.25 sec	60~1000 μsec	2~512 μsec	>15 u	N/A
Chip size	2.2 mm × 2.1 mm	N/A	N/A	4.6 mm × 4.6 mm	1.8 mm × 1.5 mm
Module size	1.7 c.c.	22 c.c.	0.05 c.c.	No Module	No Module

FES* : Functional Electrical Stimulation; BCI** : Brain Computer Interface;

DBS+: Deep Brain Stimulation; N/A : Not Availabe

FES*: functional electrical stimulation; BCI**: brain computer interface; DBS+: deep brain stimulation; N/A: not available

Fig. 16. Demonstration during PRF treatment.

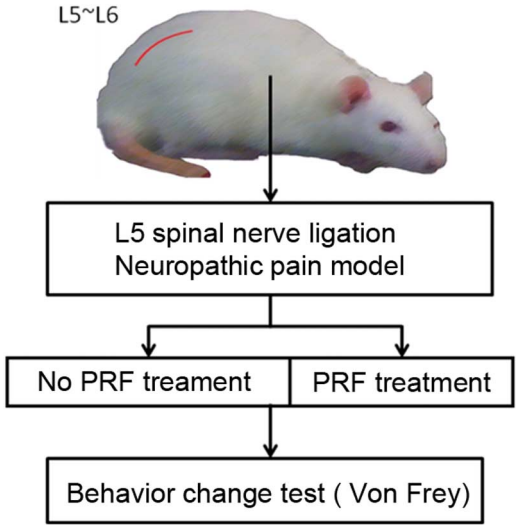

Fig. 17. Flowchart of the animal study.

Parylene C for implantation. The packaged PRF chip was then implanted into rats for the animal study. The LED inside the rat is lit once an external power source is close to the rat, demonstrating that external power is delivered to the SoC successfully as shown in Fig. 16. The animal study flowchart is shown in Fig. 17. Before the implantation, L5 nerve of the lumbar region was exposed to induce neuropathic pain by ligation. The electrode was penetrated into the transverse process and placed beside the DRG as shown in Fig. 18. Rats were grouped into a control group (2 rats) without applying PRF and an experimental group (4 rats) with a low PRF stimulation voltage of 2.8 V (biphasic), in contrast to the conventional 40 V (monophasic), for a duration of 5 min. Besides, the default 500-kHz pulse frequency, 2-Hz repetition rate, and 50-ms pulse duration were applied. Von Frey (VF) monofilaments with different bending forces were utilized to stimulate the plantar surface of the foot to test the mechanical allodynia. Specifically, when the force was applied, the animal did not withdraw its foot until it felt pain. The VF scores are defined as the average ~~threshold~~ force in grams ~~when a rat withdraws its foot~~. The paw was pressed with one of a series of VF hairs with logarithmically incrementing stiffness (0.6, 1, 1.4, 2, 4, 8, 10, 15 and 26 g, presented perpendicular to the plantar surface (5–6 s for each hair). The 50% withdrawal threshold was determined using Dixon's up-down method [31].

Therefore, a high VF score indicates high ~~pain tolerance~~. All animals were tested before surgery to collect their baseline

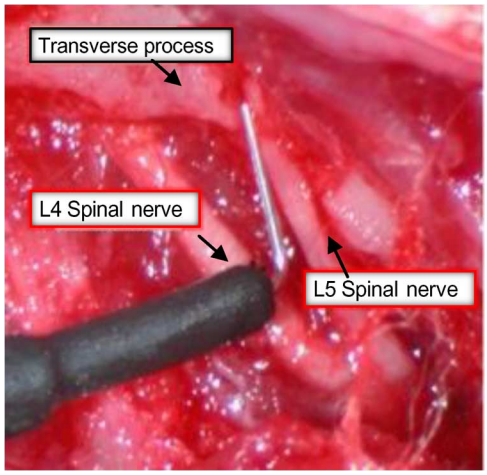

Fig. 18. Placement of stimulation electrodes on the L5.

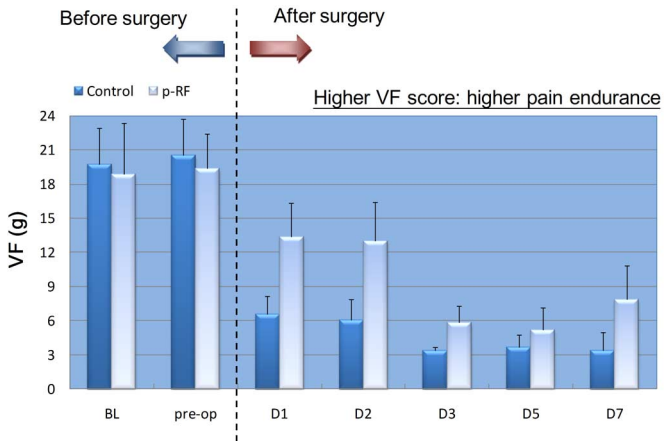

Fig. 19. Experimental results of VF score change before and after PRF stimulation to DRG.

values and were allowed to recover from surgical trauma before resuming the test on days 1, 2, 3, 5, and 7 to evaluate the threshold values of both groups. The baseline values of both groups were around 20 g before surgery and decreased after surgery (Fig. 19). Since the L5 nerve of the lumbar region was exposed to induce neuropathic pain by ligation for both groups, the baseline of VF drops after surgery. However, the experimental group with PRF stimulation consistently had higher pain tolerance than the control group without PRF stimulation. Experimental results clearly demonstrate the 3–7 days effectiveness of PRF treatment for pain relief on the DRG.

V. Conclusion

This paper has successfully demonstrated that implanted CMOS SoC stimulating DRG with 1.4-V, 500-kHz PRF could significantly reduce SNL-induced mechanical allodynia for 3–7 days. To the best of our knowledge, this device is the only batteryless SoC-based implantable stimulator whose effectiveness is demonstrated by an animal study. It is assumed that the electric field rather than temperature is responsible for the pain relief observed in clinical practice. Its effectiveness is demonstrated by observing the behavior of rats receiving localized biphasic stimulus to the DRG of the lumbar nerve. The implantation rat has lived for six months. Moreover, the direct evidence can prove the effectiveness of PRF is under study by means of immunohistochemistry.

Acknowledgment

The authors would like to thank the National Chip Implementation Center (CIC), Taiwan, for chip fabrication. They would also like to thank C.-H. Chang, Y.-C. Tsai, Prof. W.-P. Shih, Prof. Y.-J. Yang, and Prof. M.-J. Kao for helpful discussions.

References

[1] C. J. Woolf and R. J. Mannion, "Neuropathic pain: Aetiology, symptoms, mechanisms, and management," *Lancet*, vol. 353, no. 9168, pp. 1959–1964, Jun. 1999.

[2] R. A. Deyo, S. K. Mirza, and B. I. Martin, "Back pain prevalence and visit rates—Estimates from US national surveys, 2002," *Spine*, vol. 31, no. 23, pp. 2724–2727, Nov. 2006.

[3] L. G. Hart, R. A. Deyo, and D. C. Cherkin, "Physician office visits for low back pain. Frequency, clinical evaluation, and treatment patterns from a U.S. national survey," *Spine*, vol. 20, no. 1, pp. 11–19, Jan. 1995.

[4] N. Bogduk and B. McGuirk, *Medical Management of Acute Chronic Low Back Pain: An Evidence-Based Approach*. New York: Elsevier, 2002, ch. 1.

[5] J. M. Zhang, X. J. Song, and R. H. LaMotte, "Enhanced excitability of sensory neurons in rats with cutaneous hyperalgesia produced by chronic compression of the dorsal root ganglion," *J. Neurophysiol.*, vol. 82, pp. 3359–3366, Dec. 1999.

[6] J. M. Zhang, H. Li, and S. J. Brull, "Perfusion of the mechanically compressed lumbar ganglion with lidocaine reduces mechanical hyperalgesia and allodynia in the rat," *J. Neurophysiol.*, vol. 84, pp. 798–805, Aug. 2000.

[7] Z. Xiang, Y. Xiong, N. Yan, X. Li, Y. Mao, X. Ni, C. He, R. H. LaMotte, G. Burnstock, and J. Sun, "Functional up-regulation of P2X 3 receptors in the chronically compressed dorsal root ganglion," *Pain*, vol. 140, pp. 23–34, Nov. 2008.

[8] K. Malik and H. T. Benzon, "Radiofrequency applications to dorsal root ganglia: A literature review," *Anesthesiology*, vol. 109, no. 3, pp. 527–542, Sep. 2008.

[9] P. Verrills, B. Mitchell, D. Vivian, and C. Sinclair, "Peripheral nerve stimulation: A treatment for chronic low back pain and failed back surgery syndrome?," *Neuromodulation*, vol. 12, no. 1, pp. 68–75, Jan. 2009.

[10] M. Sluijter, E. Cosman, and I. Rittman, "The effects of pulsed radiofrequency field applied to the dorsal root ganglion—A preliminary report," *Pain Clin.*, vol. 11, no. 2, pp. 109–117, 1998.

[11] R. Melzack and P. D. Wall, "Pain mechanisms: A new theory," *Science*, vol. 150, no. 699, pp. 971–979, Nov. 1965.

[12] J. Sandkuhler, J. G. Chen, G. Cheng, and M. Randic, "Low-frequency stimulation of afferent Adelta-fibers induces long-term depression at primary afferent synapses with substantia gelatinosa neurons in the rat," *J. Neurosci.*, vol. 17, no. 16, pp. 6483–6491, Aug. 1997.

[13] P. Richebe, J. P. Rathmell, and T. J. Brennan, "Immediate early genes after pulsed radiofrequency treatment: Neurobiology in need of clinical trials," *Anesthesiology*, vol. 102, no. 1, pp. 1–3, Jan. 2005.

[14] S. Hagiwara, H. Iwasaka, N. Takeshima, and T. Noguchi, "Mechanisms of analgesic action of pulsed radiofrequency on adjuvant-induced pain in the rat: Roles of descending adrenergic and serotonergic systems," *Eur. J. Pain*, vol. 13, no. 3, pp. 249–252, Mar. 2009.

[15] R. Munglani, "The longer term effect of pulsed radiofrequency for neuropathic pain," *Pain*, vol. 80, no. 1–2, pp. 437–439, Mar. 1999.

[16] J. Van Zundert, S. Brabant, E. Van de Kelft, A. Vercruyssen, and J. P. Van Buyten, "Pulsed radiofrequency treatment of the Gasserian ganglion in patients with idiopathic trigeminal neuralgia," *Pain*, vol. 104, pp. 449–452, Aug. 2003.

[17] J. Van Zundert, J. Patijn, A. Kessels, I. Lame, H. van Suijlekom, and M. van Kleef, "Pulsed radiofrequency adjacent to the cervical dorsal root ganglion in chronic cervical radicular pain: A double blind sham controlled randomized clinical trial," *Pain*, vol. 127, pp. 173–182, Jan. 2007.

[18] D. Byrd and S. Mackey, "Pulsed radiofrequency for chronic pain," *Current Pain Headache Rep.*, vol. 12, no. 1, pp. 37–41, Feb. 2008.

[19] P. Richebe, J. P. Rathmell, and T. J. Brennan, "Immediate early genes after pulsed radiofrequency treatment: Neurobiology in need of clinical trials," *Anesthesiology*, vol. 102, no. 1, pp. 1–3, Jan. 2005.

[20] T. T. Simopoulos, J. Kraemer, J. V. Nagda, M. Aner, and Z. H. Bajwa, "Response to pulsed and continuous radiofrequency lesioning of the dorsal root ganglion and segmental nerves in patients with chronic lumbar radicular pain," *Pain Physic.*, vol. 11, no. 2, pp. 137–144, Mar./Apr. 2008.
[21] M. L. Lin, C. H. Chang, C. W. Lin, H. W. Chiu, Y. R. Wen, and S. H. Lin, "Implantable pulsed-RF on dorsal root ganglion for treatment of neuropathic pain—Animal study," presented at the WIP, New York, 2009.
[22] C. H. Chen, R. Z. Hwang, L. S. Huang, S. Lin, H. C. Chen, Y. C. Yang, Y. T. Lin, S. A. Yu, Y. H. Wang, N. K. Chou, and S. S. Lu, "A wireless bio-MEMS sensor for C-reactive protein detection based on nanomechanics," in *Proc. IEEE Int. Solid-State Circuits Conf.*, Feb. 2006, pp. 376–377.
[23] C. Peters, O. Kessling, F. Henrici, M. Ortmanns, and Y. Manoli, "CMOS integrated highly efficient full wave rectifier," in *Proc. IEEE Intl. Symp. Cir. Syst.*, 2007, pp. 2415–2418.
[24] S. Guo and H. Lee, "An efficiency-enhanced CMOS rectifier with unbalanced-biased comparators for transcutaneous-powered high-current implants," *IEEE J. Solid-State Circuits*, vol. 44, no. 6, pp. 1796–1804, Jun. 2009.
[25] C. H. Chen, R. Z. Hwang, L. S. Huang, S. M. Lin, H. C. Chen, Y. C. Yang, Y. T. Lin, S. A. Yu, Y. S. Lin, Y. H. Wang, N. K. Chou, and S. S. Lu, "A wireless bio-MEMS sensor for C-reactive protein detection based on nanomechanics," *IEEE Trans. Biomed. Eng.*, vol. 56, no. 2, pp. 462–470, Feb. 2009.
[26] K. N. Leung and P. K. T. Mok, "A sub-1-V 15-ppm/C CMOS bandgap voltage reference without requiring low threshold voltage device," *IEEE J. Solid-State Circuits*, vol. 37, no. 4, pp. 526–530, Apr. 2002.
[27] RestoreUltra Technical Manual. 2007. [Online]. Available: http://professional.medtronic.com/devices/restoreultra/overview
[28] G. E. Loeb, F. J. Richmond, and L. L. Baker, "The BION devices: Injectable interfaces with peripheral nerves and muscles," *Neurosurg. Focus*, vol. 20, no. 5, May 2006.
[29] M. Ghovanloo and K. Najafi, "A modular 32-site wireless neural stimulation microsystem," *IEEE J. Solid-State Circuits*, vol. 39, no. 12, pp. 2457–2466, Dec. 2004.
[30] J. Lee, H. Rhew, D. Kipke, and M. Flynn, "A 64 channel programmable closed-loop deep brain stimulator with 8 channel neural amplifier and logarithmic ADC," in *Proc. Symp. VLSI Circuits Dig. Tech. Papers*, 2008, pp. 76–77.
[31] S. R. Chaplan, F. W. Bach, J. W. Pogrel, J. M. Chung, and T. L. Yaksh, "Quantitative assessment of tactile allodynia in the rat paw," *J. Neurosci. Meth.*, vol. 53, no. 1, pp. 55–63, Jul. 1994.

Hung-Wei Chiu (M'09) was born in Taipei, Taiwan. He received the B.S. degree in electrical engineering from National Chia-Tung Univeristy in 1998, and the M.S. and Ph.D. degrees in electrical engineering from National Taiwan University in 2000 and 2003, respectively.

In 2004, he joined the Taiwan Semiconductor Manufacturing Company (TSMC) as a Designer with the Mixed-Mode and RF Library Division. Since then, he has worked in the area of the automation of mixed-mode and RF circuit design. In 2005, he joined the Department of Electronic Engineering and Graduate Institute of Computer and Communication Engineering, National Taipei University of Technology, Taipei, where he is currently an Assistant Professor. His research interests are in the areas of radio-frequency integrated circuits, wireless power electronics, and implantable biomedical microsystems.

Mu-Lien Lin is currently pursuing the Ph.D. degree at the Graduate of Institute of Biomedical Engineering, National Taiwan University, working on research in biomedical microsensors and personal e-health systems.

After completing resident training of anesthesia in Veterans General Hospital, Taipei; National Taiwan University Hospital, Taipei; and Ho-Ping City Hospital, Taipei, respectively, he had applied for fellowship at the Medical Center of the University of Southern California in 1990, where he had learned more about advanced pain management in addition to general anesthesia, including various high technical nerve blocks, and completed a project of "Neurotoxicity of intraspinal analgesics." After coming back to Taiwan, he has been assigned as Chief of Anesthesia and Director of Pain Center in Taipei City Hospital Zhongxing Branch and has done a lot of work on pain clinic and research. For 20 years, his interest is involved in the field of spinal pain, He is also deeply involved in a Spine Team at the Department of Orthopedic Surgery, NTUH.

Mr. Liu is also a member of the American Society of Anesthesiologists, International Association for the Study of Pain, World Institute for Pain, Taiwan Society of Anesthesiologiests, Taiwan Society of Cardiovascular Anesthesia, and the Chinese Association for the Study of Pain.

Chii-Wann Lin received the B.S. degree in electrical engineering from National Cheng-Kung University in 1984, the M.S. degree from the Graduate Institute of Biomedical Engineering, National Yang-Ming University, in 1986, and the Ph.D. degree from Case Western Reserve University, Cleveland, OH, in 1993.

He then joined the Center for Biomedical Engineering, College of Medicine, National Taiwan University, from 1993 to 1998. Currently, he is a Professor in the Graduate Institute of Biomedical Engineering and holds joint appointments in the Department of Electrical Engineering and Institute of Applied Mechanics, National Taiwan University.

Prof. Lin is a member of the IEEE Engineering in Medicine and Biology Society, International Federation for Medical and Biological Society, Taiwan Association of Chemical Sensors, and the Chinese Biomedical Engineering Society. He is the President of the Taiwan Association of Chemical Sensors from 2008 to 2010. His research interests include biomedical microsensors, optical biochip, surface plasmon resonance, bioplasmonics, nanomedicine, and personal e-health systems.

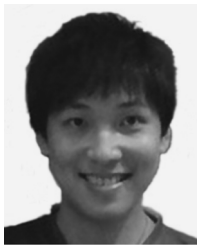

I-Hsiu Ho was born in Taoyuan, Taiwan. He received the B.S. and M.S. degrees from National Taipei University of Technology, in 2008 and 2010, respectively.

In 2004, he joined the Elite Semiconductor Memory Technology, Inc., Taiwan. His research interest is in the area of wireless power electronics.

Wei-Tso Lin received the M.S. degree from the Institute of Biomedical Engineering, National Taiwan University, Taipei, Taiwan, in 2010, where he is currently pursuing the Ph.D. degree in biomedical engineering.

His research interests include pulsed radio-frequency stimulation of pain.

Po-Hsiang Fang was born in Taipei, Taiwan. He received the B.S. and M.S. degrees in electrical engineering from National Taiwan University in 2007 and 2009, respectively.

In 2009, he joined Novatek Microelectronics Corp., Taiwan. His research interests are analog-to-digital converters and analog circuit design.

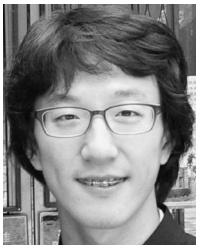

Yi-Chin Lee was born in Taipei, Taiwan. He received the B.S. degree in mechanical engineering and the M.S. degree in electrical engineering from National Taiwan University in 2006 and 2009, respectively.

In 2009, he joined Compal Electronics, Inc., Taiwan. His research interest is in the area of digital circuit design.

Yeong-Ray Wen received the M.D. degree from Medical School, China Medical University, Taichung, Taiwan, and the Ph.D. degree from the Graduate Institute of Clinical Medicine, Taipei Medical University, Taipei, Taiwan, in 2009.

He completed his resident and subspecialist training in the Department of Anesthesiology, National Taiwan University Hospital. He became a Postdoctoral Research Fellow in the Sensory Plasticity Laboratory of the Pain Research Center, Department of Anesthesiology, Brigham and Women Hospital, Harvard Medical School, from 2004 to 2005. Currently, he is an Attending Doctor in the Department of Anesthesiology, Shin-Kong Wu Ho-Su Memorial Hospital, Taipei, Taiwan, where he specializes in clinical anesthesia and pain management, especially in neuropathic pain and hospice care. His research interests include the fields of various animal pain models, mechanisms of acupuncture analgesia, spinal nociceptive sensitization, spinal glial activation, and morphine tolerance.

Shey-Shi Lu (S'89–M'91–SM'99) received the B.S. degree in electrical engineering from National Taiwan University in 1985, the M.S. degree in electrical engineering from Cornell University, Ithaca, NY, in 1988, and the Ph.D. degree in electrical engineering from the University of Minnesota in 1991.

His Master's thesis was related to the planar-doped barrier hot electron transistor while his Ph.D. thesis focused on the uniaxial stress effect on AlGaAs/GaAs quantum well/barrier structures. His current research interests are in the areas of complementary metal–oxide semiconductor (CMOS) biotechnology and CMOS radio-frequency integrated circuits. During 1990, he was a Research Aide at the IBM T.J. Watson Research Center, working on the diffusion ohmic contact. He joined the Department of Electrical Engineering, National Taiwan University, in 1991 as an Associate Professor and was promoted to Full Professor in 1995.

Dr. Liu received the Outstanding Research Award from the National Science Council in 2009, Distinguished Engineering Professor Award from the Chinese Institute of Electrical Engineering in 2006, and Fu Szu-Nien Award from the National Taiwan University in 2005.